RSC Advances

PAPER

View Article Online
View Journal | View Issue

Cite this: *RSC Adv.*, 2022, **12**, 16798

Ferric ion detection mechanism of a dicarboxylic cellulose nanocrystal and a 7-amino-4-methylcoumarin based fluorescent chemosensor

Xiaozheng Sun, *[a] Jianye Li,[a] Qiang He,[b] Yanhua Xue,[a] Yu Bai,[a] Yuyao Yang,[a] Xiaogang Wang,[a] Sun Wang[a] and Rui Li[a]

Received 9th April 2022
Accepted 1st June 2022

DOI: 10.1039/d2ra02303b

rsc.li/rsc-advances

As one of Earth's most widely distributed and abundant elements, iron impacts the natural environment and biological systems. Therefore, developing a simple, rapid, and accurate Fe^{3+} detection method is vital. Fluorescent dicarboxylic cellulose nanocrystals (FDCN) with selective quenching of Fe^{3+} were synthesized using 7-amino-4-methylcoumarin (AMC), and dicarboxylic cellulose nanocrystals (DCN) prepared by sequential periodate–chlorite oxidation. The sensing characteristics and detection mechanism of FDCN for Fe^{3+} were studied by fluorescence spectrophotometry, Fourier-transform infrared spectroscopy (FTIR), the Stern–Volmer equation, Job's plot method, and the Benesi–Hildebrand equation. The results showed that FDCN was highly selective for Fe^{3+}, and other metal ions did not reduce the selectivity. High sensitivity with a detection limit of 0.26 μM and a Stern–Volmer quenching constant of 0.1229 were also achieved. The coordination between Fe^{3+} and the carboxylic, hydroxyl, and amide groups on the surface of FDCN and the carbonyl of coumarin lactones to form FDCN/Fe^{3+} complexes prevented the intramolecular charge transfer (ICT) process and led to the fluorescence quenching of FDCN. EDTA restored the fluorescence emission of quenched FDCN. The complexation stoichiometry of Fe^{3+} to FDCN was 1 : 1, and the association constant was 3.23×10^4 M^{-1}. The high hydrophilicity, sensitivity, and selectivity of FDCN for Fe^{3+} make the chemosensor suitable for Fe^{3+} trace detection in drinking water and biology.

Introduction

Iron ions are widely distributed in nature and are a vital nutrient for animal and plant growth and human health.[1] However, excessive consumption of Fe^{3+} damages human tissues, leading to functional impairment of organs such as the kidneys, liver, and heart. Studies also show that excessive Fe^{3+} intake can easily cause cancer and neurological diseases, such as Alzheimer's disease and Parkinson's disease.[2–4] Meanwhile, Fe^{3+} deficiency can easily cause tissue or cell hypoxia, leading to serious health problems.[5,6] Therefore, it is crucial to develop a method that can selectively identify trace Fe^{3+} in the most consumed substances – especially water. Fe^{3+} detection methods mainly include atomic absorption spectrometry (AAS)[7,8] inductive coupling, plasma mass spectrometry (ICP-MS),[9] and electrochemical methods.[10] However, these methods have drawbacks such as complicated detection processes and expensive instrumentation. Fluorescence detection has become the preferred method for detecting Fe^{3+} in water because of its high sensitivity, selectivity, and ease of detection.[11] Many fluorescent probes or chemosensors for detecting Fe^{3+} have been developed.[12–15] However, some fluorescent probes still have limitations such as toxicity, poor hydrophilicity, and low biocompatibility. Hence, there is still a need for further research to develop Fe^{3+} fluorescent probes.

Among numerous materials, nanocellulose is an attractive material for synthesizing fluorescent probes due to its carbon neutrality,[16] low cytotoxicity,[17] good biocompatibility, and availability in a vast source of raw materials.[18] Various studies have proven nanocellulose as a suitable matrix material for the synthesis of fluorescent probes.[19–22] For instance, the immobilization of fluorescent dyes on nanocellulose has been demonstrated to improve the performance of fluorescent probes.[23,24] Elsewhere, citrate-based fluorophore-modified cellulose nanocrystals (CF-CNC) were prepared with sulfuric acid hydrolysis of citric acid/cysteine-treated microcrystalline celluloses. The CF-CNC exhibited typical fluorescence characteristics, including a high quantum yield of 83%, good photostability, and a selective quenching effect toward Fe^{3+} ions.[25] Xue *et al.* mixed citric acid, ethylenediamine, and cellulose nanofibrils prepared by 2,2,6,6-tetramethylpiperidin-1-yl-oxyl (TEMPO)-mediated oxidation and processed them with a one-step hydrothermal treatment. Fluorescent cellulose nanofibrils were obtained

[a]College of Engineering, Northeast Agricultural University, No. 600 Changjiang Street, Harbin, 150030, China. E-mail: sxz1976@hotmail.com
[b]College of Mechanical Engineering, Jiamusi University, No. 258 Xuefu Street, Jiamusi, 154007, China

through amide bonds from the grafted carbon quantum dots. The fluorescent cellulose nanofibrils demonstrated significant selectivity toward Fe^{3+} ions.[26] Py-CNC were prepared by grafting pyrene onto cellulose nanocrystals (CNC) prepared by sulfuric acid hydrolysis. The Py-CNC had excellent selectivity for Fe^{3+} over a wide linear concentration range, and the fluorescent emission was stronger than that of pyrene alone.[24]

The process of periodate oxidation is safer and simpler than sulfuric acid hydrolysis. Also, the content of carboxyl groups on dicarboxylic cellulose nanocrystals (DCN) prepared by sequential periodate–chlorite oxidation is higher than that of cellulose nanofibrils prepared by TEMPO-mediated oxidation.[18] Furthermore, the high carboxyl group content results in better dispersibility in water and easy chemical modification. Fluorescent dicarboxylic cellulose nanocrystals (FDCN) were prepared by attaching 7-amino-4-methylcoumarin (AMC) to DCN prepared by sequential periodate–chlorite oxidation under 4-(4,6-dimethoxy-1,3,5-triazin-2-yl)-4-methylmorpholinium chloride (DMTMM) catalysis. Many studies have shown that coumarin derivatives containing amide bonds exhibit selective fluorescence quenching of Fe^{3+}.[27–29] Although the fluorescent CNC prepared by grafting AMC onto CNC derived from sulfuric acid hydrolysis also contained amide bonds, and they exhibited a selective fluorescence quenching effect on Cu^{2+}.[30] To the best of our knowledge, there is no relevant report on detecting metal ions by FDCN, and the metal ion binding properties of FDCN are still unclear.

Hence, the objective of this study was to determine the fluorescence properties of FDCN and its detection mechanism for metal ions in water. The experimental results showed that FDCN exhibited a selective fluorescence quenching effect on Fe^{3+} ions. The sensing characteristics and detection mechanism of FDCN for Fe^{3+} were studied by fluorescence spectrophotometry, Fourier-transform infrared spectroscopy (FTIR), the Stern–Volmer equation, Job's plot method, and the Benesi–Hildebrand equation.

Experimental

Materials and characterizations

Materials. All reagent-grade chemicals were used as received and without further purification. All chemical stock solutions were prepared with deionized water in all experiments. FDCN was prepared with the synthesis method of FCNC-5 as previously described.[22] The chemicals that were used in the experiments include the following: cadmium sulfate ($3CdSO_4 \cdot 8H_2O$), lithium sulfate ($Li_2SO_4 \cdot H_2O$), zinc sulfate ($ZnSO_4 \cdot 7H_2O$), copper(II) sulfate ($CuSO_4 \cdot 5H_2O$), iron(II) sulfate ($FeSO_4 \cdot 7H_2O$), silver sulfite (Ag_2SO_3), manganese(II) sulfate ($MnSO_4$), cobalt(II) chloride hexahydrate ($CoCl_2 \cdot 6(H_2O)$), nickel(II) chloride ($NiCl_2 \cdot 6H_2O$), barium chloride dihydrate ($BaCl_2 \cdot 2H_2O$), lead(II) nitrate ($Pb(NO_3)_2$), magnesium nitrate hexahydrate ($Mg(NO_3)_2 \cdot 6H_2O$), and iron(III) chloride ($FeCl_3$).

Characterisations. The infrared spectrum of absorption or emission of the samples was recorded and analyzed using the Fourier-transform infrared (FTIR) spectrometer (mod. Nicolet iS50 FTIR, Thermo Fisher Scientific (Pty) Ltd, China). The fluorescence of the samples was recorded on a fluorescence spectrophotometer (mod. F-7100, Hitachi (Pty) Ltd, Japan) with the slit set to 5 nm/5 nm. The excitation wavelengths of AMC and FDCN were 350 nm and 335 nm, respectively.

Selectivity experiment of FDCN toward metal ions

Thirteen common metal ions were selected to explore the fluorescence response of FDCN. Ten mg of FDCN powder were placed in 10 mL of 1 mM Ag^+, Ni^{2+}, Mg^{2+}, Zn^{2+}, Fe^{3+}, Cu^{2+}, Pb^{2+}, Mn^{2+}, Fe^{2+}, Co^{2+}, Cd^{2+}, Li^+, and Ba^{2+} ion solutions, respectively. The mixture was then uniformly dispersed using sonication (mod. KQ-200KDE, Kunshan Ultrasonic Instruments (Pty) Ltd, China) for 5 min. 2 mL of the dispersion solution was pipetted into a quartz cuvette, and its fluorescence spectrum was measured at room temperature. All experiments were performed in triplicates.

Competition experiments of metal ions

For the practical application of probes, most samples contain a variety of metal ions, and it is necessary to study the change in the selective quenching ability of FDCN to specific metal ions in the presence of other metal ions. Ten mg of FDCN powder were placed in 10 mL of 1 mM Ag^+, Ni^{2+}, Mg^{2+}, Zn^{2+}, Cu^{2+}, Pb^{2+}, Mn^{2+}, Fe^{2+}, Co^{2+}, Cd^{2+}, Li^+, Ba^{2+} ions and 1 mM Fe^{3+} ions coexistence solutions, respectively. Ultrasonic dispersion was performed for 5 min to ensure even dispersion. 2 mL of the dispersion solution was removed using a pipette and placed in a quartz cuvette, and the fluorescence spectra were recorded at room temperature. Experiments were performed in triplicates.

Fluorescent titration experiments

Fluorescent titration experiments were performed at various concentrations of Fe^{3+} to obtain insight into the binding properties of FDCN to Fe^{3+} ions. The effect of Fe^{3+} concentration on the fluorescence intensity of FDCN was studied in the 1–500 μM range. The Fe^{3+} concentration was in the range of 1–5 μM in the Stern–Volmer fluorescence quenching experiments. The Stern–Volmer eqn (1) was used to explore the nature of the quenching process in the complexation of metal ions.[31]

$$\frac{F_0}{F} = 1 + K_{SV}[Q] \quad (1)$$

where F and F_0 are the fluorescence intensities of FDCN in the presence and absence Fe^{3+} ions. K_{SV} is the Stern–Volmer fluorescence quenching constant, and Q is the Fe^{3+} concentration (μM).

The association stoichiometry between FDCN and Fe^{3+} was determined using the Job's plot method.[12] The addition ratio of Fe^{3+} and FDCN was maintained at 0–1. The total concentration was kept at 10 μM while the molar ratio of FDCN to Fe^{3+} was gradually changed. The fluorescence intensities of the mixture with different addition ratios were recorded, and the Job's plot was made by taking eqn (2) as the ordinate eqn (3) as the abscissas.[32]

$$XF_0 - F \quad (2)$$

$$[Fe^{3+}]/([FDCN] + [Fe^{3+}]) \quad (3)$$

Benesi–Hildebrand eqn (4) calculated the association constant (K_{ac}).[33]

$$\frac{1}{F_0 - F} = \frac{1}{K_{ac}(F_0 - F_{min})[Fe^{3+}]^n} + \frac{1}{F_0 - F_{min}} \quad (4)$$

where F and F_0 are the fluorescence intensities of FDCN at a wavelength of 440 nm in the presence and absence of Fe^{3+} ions, F_{min} is the minimum fluorescence intensity in the titration experiment of FDCN and Fe^{3+}, and n is the binding stoichiometry of FDCN and Fe^{3+} ions.

Results and discussion

Selectivity experiments of FDCN for metal ions

Thirteen common metal ions were selected to explore the fluorescence response of FDCN. Fig. 1 shows the relative fluorescence intensity of FDCN at an excitation wavelength of 335 nm and an emission wavelength of 440 nm in different metal ion solutions. In F/F_0, F, and F_0 are the fluorescence intensities of FDCN in the presence and absence of metal ions, respectively. Different metal ions caused different degrees of change in the fluorescence intensity of FDCN. The addition of Ag^+, Li^+, Ba^{2+}, and Fe^{2+} slightly increased the fluorescence intensity of FDCN. The fluorescence intensity of FDCN did not change significantly in the presence of Ni^{2+} and Mg^{2+}. The addition of Zn^{2+}, Cu^{2+}, Pb^{2+}, Mn^{2+}, Co^{2+}, Cd^{2+}, or Ba^{2+} slightly attenuated the fluorescence intensity of FDCN. The fluorescence intensity was significantly reduced in the presence of Fe^{3+}, and fluorescence quenching occurred. These results show that only Fe^{3+} had a substantial fluorescence quenching effect on FDCN.

Competition of metal ions

Most actual samples contain a variety of metal ions; therefore, it is necessary to explore the change in the selective quenching effect of FDCN on Fe^{3+} in the presence of other metal ions. Fig. 2 shows the effects of different metal ions on Fe^{3+} detection by FDCN. After adding other metal ions, the response of FDCN to Fe^{3+} did not change significantly. Also, the quenching effect was not greatly affected, and the fluorescence intensity remained unchanged. This result shows that other metal ions have little effect on the quenching of FDCN to Fe^{3+}, and their potential interference can be ignored. Most importantly, this outcome shows that FDCN had a highly selective quenching effect on the Fe^{3+} ions.

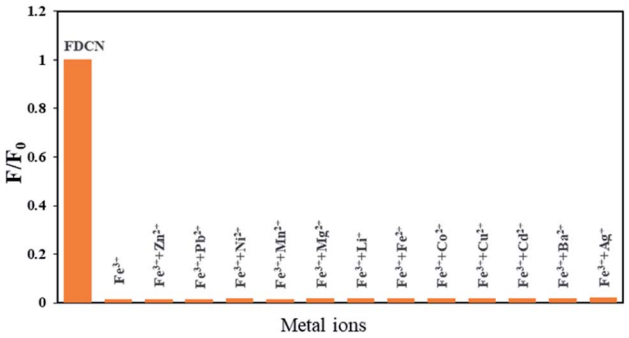

Fig. 2 Effects of different metal ions on the Fe^{3+} detection of FDCN.

Five electrons occupy five orbitals in a spin–parallel manner in the free ionic state because the outer electron orbital of the Fe^{3+} ion has a $3d^5$ structure, and there are five under-filled electron orbitals. When Fe^{3+} encounters FDCN, the electrons are rearranged to three d orbitals, forming six d^2sp^3 hybrid orbitals by vacating two d orbitals and the outer 4s and 4p orbitals. This hybrid orbital accepts six pairs of ligand electrons. Among the ions in this experiment, only Fe^{3+} can form d^2sp^3 hybrid orbitals, and the bonding affinity of d^2sp^3 hybrid orbitals is the strongest in s–p hybridization. Therefore, FDCN has a high selectivity for Fe^{3+} ions.

Fluorescence titration

Fig. 3 shows the fluorescence spectrum of FDCN with Fe^{3+} concentrations in the range of 1–500 μM. An increase in Fe^{3+} concentration decreased the fluorescence intensity of FDCN; however, the emission wavelength did not shift. Fig. 4a shows the relationship between the fluorescence intensity change ratio (F/F_0) of FDCN and Fe^{3+} concentration. F/F_0 gradually decreased with increasing Fe^{3+} concentration. When the Fe^{3+}

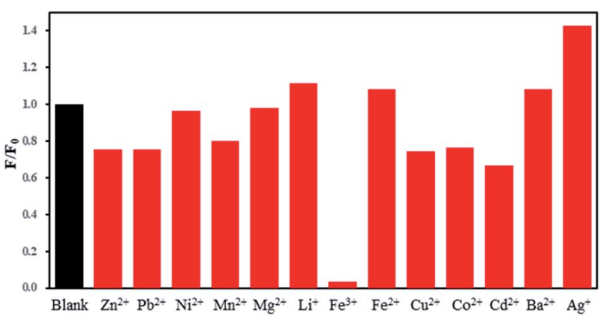

Fig. 1 Effects of different metal ions on the fluorescence intensity of FDCN.

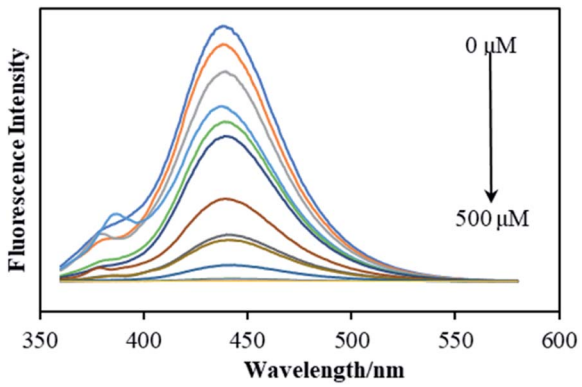

Fig. 3 Effect of Fe^{3+} concentration on the fluorescence intensity of FDCN.

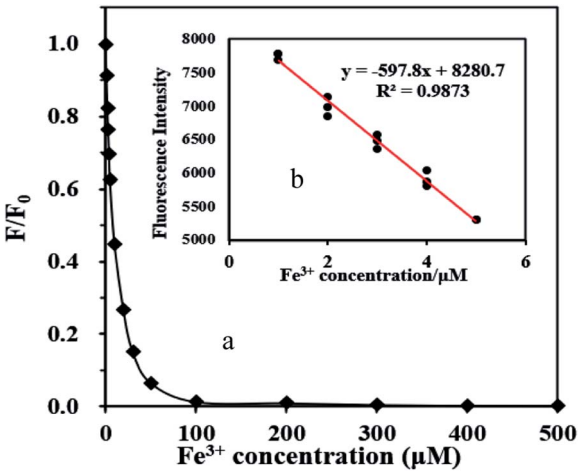

Fig. 4 Relationship between F/F_0 and Fe^{3+} concentration in the range of 1–500 μM (a), and the relationship between the fluorescence intensity and Fe^{3+} concentration (b).

concentration was 1–5 μM, there was a good linear relationship between the fluorescence intensity and Fe^{3+} concentration as shown in Fig. 4b. When the Fe^{3+} concentration was above 50 μM, the value of F/F_0 tended to be stable as the Fe^{3+} concentration was increased further. When the Fe^{3+} concentration was above 100 μM, F/F_0 approached 0 with increasing Fe^{3+} concentration.

Sensitivity studies

As shown in Fig. 5, the fluorescence quenching of FDCN by Fe^{3+} conformed to the Stern–Volmer eqn (1), indicating that it was a dynamic quenching process. There was a good linear relationship between F_0/F and Fe^{3+} concentrations in the range of 1–5 μM, and the fitted linear equation was as in eqn (5) as follows:

$$F_0/F = 0.1229x + 0.9596 \ (R^2 = 0.9832) \quad (5)$$

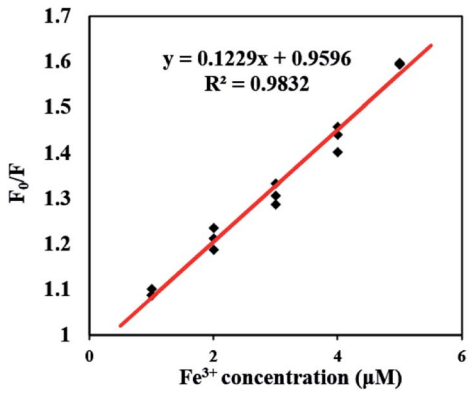

Fig. 5 Change fluorescence intensity of FDCN with the increasing Fe^{3+} concentration (1 to 5 μM).

The Stern–Volmer fluorescence quenching constant was 0.1229, larger than those reported by Chen *et al.* (0.0379)[25] and Zhang *et al.* (0.0336).[24] The result shows that the probe in this study has a higher sensing sensitivity to Fe^{3+} ions. The detection limit of Fe^{3+} was determined to be 0.26 μM using the $3s/k$ equation. The determination limit of Fe^{3+} was 0.77 μM using the $6s/k$ equation. The symbol s is the standard deviation of the blank samples for 10 times, k is the slope of the line mentioned in Fig. 4b.[12,34] As shown in Table 1, the detection limit of this study reached a low level, far below the limit of Fe^{3+} concentration in drinking water of 5.357 μM compared with other research results.[32] Therefore, the fluorescence sensor can detect Fe^{3+} in drinking water rapidly.

Bozkurt *et al.* showed that when the Fe^{3+} concentration reached 20 mM, the AMC fluorescence intensity decreased by approximately 40%.[12] In this study, the fluorescence quenching effect of FDCN exceeded 90% when the Fe^{3+} concentration reached 100 μM. It was proven that the detection responseability of FDCN to Fe^{3+} was higher than that of AMC. The Stern–Volmer quenching constant of AMC to Fe^{3+} was 0.0596,[12] while the quenching constant of FDCN was 0.1229. This outcome also indicates that the sensitivity of FDCN to detect Fe^{3+} was higher than that of AMC. The unreacted carboxyl groups of DCN may have influenced this result, and newly formed amide bonds in FDCN greatly enhance the selective quenching effect of FDCN on Fe^{3+} ions.

Stoichiometry determination

A Job's plot analysis was conducted to determine the association stoichiometry between FDCN and Fe^{3+}.[12] Eqn (2) showed a maximum value when the molar fraction based on eqn (3) was approximately 0.5, and the molar ratio between FDCN and Fe^{3+} ions was close to 1 : 1, indicating that the complexation stoichiometry of FDCN to Fe^{3+} ions was 1 : 1 (Fig. 6).

Association constant determination with Benesi–Hildebrand equation

The Benesi–Hildebrand equation was used to calculate the association constant (K_{ac}) when the binding stoichiometry for FDCN and Fe^{3+} was 1. Linear fitting was performed with $1/[Fe^{3+}]$ as the abscissa and $1/(F_0 - F)$ as the ordinate (Fig. 7). The fitting equation was found to be eqn (6) as follows:

$$y = 1.3462 \times 10^{-9}x + 4.3519 \times 10^{-5} \ (R^2 = 0.9856) \quad (6)$$

Table 1 Comparison of detection performance of nanocellulose-based fluorescence sensor for Fe^{3+}

Fluorescent sensor	K_{sv} (M^{-1})	K_{ac}(M^{-1})	LOD (μM)	Ref.
Py-CNC	3.36×10^4	3.68×10^4	1.0	24
CNF-DA	—	—	0.5	35
N-CDs	6.68×10^3	—	1.14	36
FDCN	1.229×10^5	3.23×10^4	0.26	This study

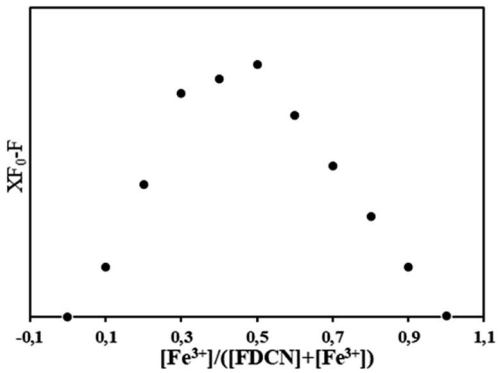

Fig. 6 Job's plot of FDCN with Fe^{3+} in water.

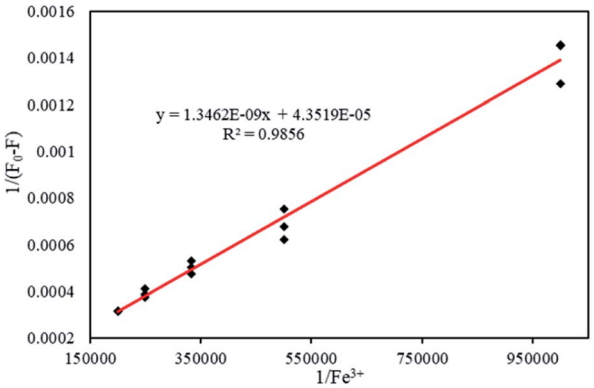

Fig. 7 Benesi–Hildebrand plot based on a 1 : 1 association stoichiometry between FDCN and Fe^{3+}.

The association constant was 3.23×10^4 M^{-1} calculated from the slope and intercept of the line. This result was higher than those reported by Zhang *et al.* (1.6×10^4 M^{-1})[32] and Chen *et al.* (2.2×10^4 M^{-1}),[27] indicating that FDCN could better recognize Fe^{3+} ions.

The mechanism of complexation between the FDCN and Fe^{3+} ions

The mechanism of complexation between FDCN and Fe^{3+} was determined using FTIR spectroscopy. Fe^{3+} was added to the FDCN dispersion and stirred for 5 min. After centrifugation, the FDCN/Fe^{3+} complex was obtained from the precipitate by freeze-drying and measured using a Fourier transform infrared spectrometer. Fig. 8 shows the FTIR spectra of AMC, DCN, FDCN, and FDCN/Fe^{3+} complexes. The analysis of FTIR spectra was referred mainly the Sadtler Handbook of Infrared Spectra.[37] After AMC was grafted onto DCN, the grafted product FDCN showed a characteristic peak of C=C at 1618 cm^{-1}, corresponding to the carbon–carbon double bond between position 3 and 4 of coumarin lactone.[38] An apparent characteristic peak was detected at 1529 cm^{-1}, corresponding to the combination of N–H deformation and C–N stretching vibration of the newly formed amido groups between the carboxyl groups of DCN and the amino groups of AMC.[37] In addition, a broad band appeared

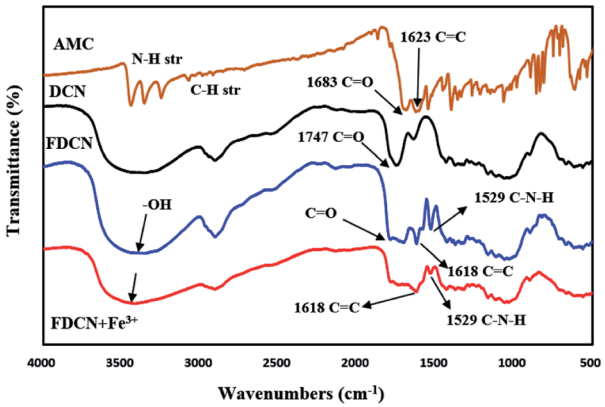

Fig. 8 FTIR spectrum of AMC, DCN, FDCN, and FDCN + Fe^{3+}.

between 1700 and 1786 cm^{-1} of FDCN FTIR, corresponding to the overlapping peaks formed by the carbonyl groups of DCN, amide, and AMC.[37] Thus, it can be deduced that AMC was grafted onto DCN through an amide bond. Owing to the amidation reaction of the amino group, the electron-pushing ability of the amino group at the position 7 was weakened, and the fluorescence emission of FDCN was blue-shifted and weakened relative to AMC (Fig. 9).

After adding Fe^{3+} ions, the stretching vibration of the hydroxyl groups (–OH) at 3420 cm^{-1} changed from a strong and sharp absorption band to a mild and broad band. This result shows that the hydroxyl groups were involved in the complexation with Fe^{3+} ions.[24] The characteristic peak of the amide bonds at 1529 cm^{-1} was also weakened from a strong and sharp absorption peak to a weak peak, indicating that the amide bonds were also involved in the complexation with Fe^{3+} ions (N–Fe bonds).[35] The characteristic broad band of carbonyl at 1700–1786 cm^{-1} also changed significantly, indicating that carbonyl groups are also important functional groups for complexation with Fe^{3+} ions.[35] According to the results, the fluorescence quenching mechanism of Fe^{3+} on FDCN was determined (Fig. 10).

The fluorescence emission mechanism of AMC involves intramolecular charge transfer (ICT).[39,40] After Fe^{3+} was added to

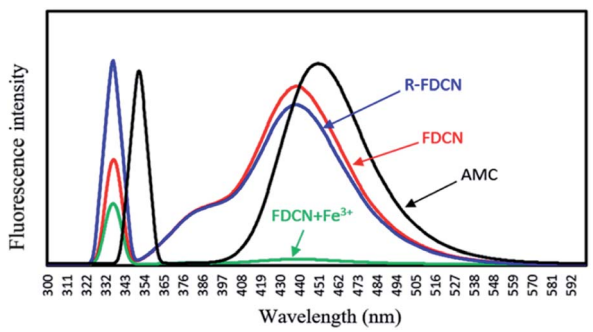

Fig. 9 Fluorescence spectra of AMC, FDCN, FDCN + Fe^{3+} and R-FDCN (FDCN + Fe^{3+}+EDTA) (AMC concentration was 2×10^{-4} M, corresponding to the grafting concentration of AMC on FDCN).

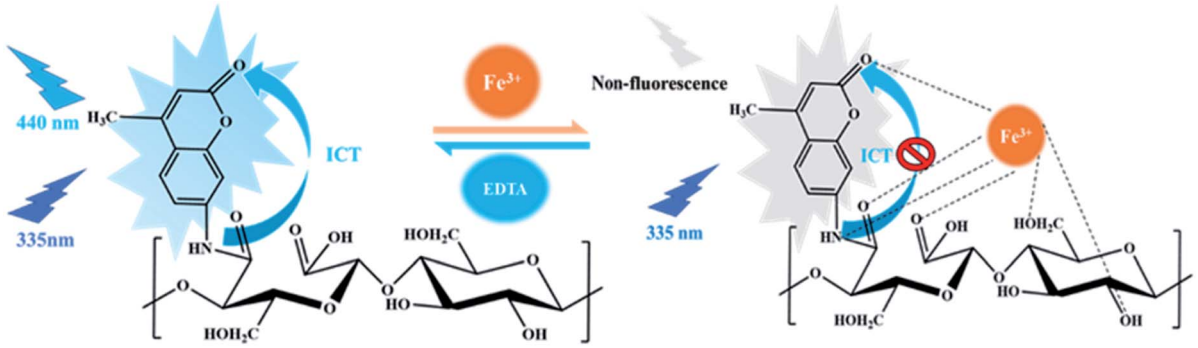

Fig. 10 The mechanism of complexation between the FDCN and Fe^{3+} ions.

the FDCN dispersion solution, the Fe^{3+} ions complexed with the amide groups and coumarin lactone carbonyl of FDCN and carbonyl and hydroxyl groups of DCN to form a coordination compound, which prevented the ICT process and led to fluorescence quenching of FDCN. After adding EDTA to the mixture, because the binding affinity of EDTA was greater than that of FDCN, the Fe^{3+} ions were removed by EDTA to form a coordination compound, and the ICT process of FDCN was restored. The fluorescence emission capability of the chemosensor was also restored (Fig. 9 R-FDCN).

Conclusions

A highly selective and sensitive fluorescent chemosensor was synthesized for Fe^{3+} based on dicarboxylic cellulose nanocrystals and 7-amino-4-methylcoumarin. The detection mechanism of the chemosensor for Fe^{3+} was evaluated using FTIR spectroscopy. The coordination between Fe^{3+} and the amide groups, the carboxyl and hydroxyl groups on the surface of FDCN, and the carbonyl of coumarin lactones to form FDCN/Fe^{3+} complexes prevented the ICT process and led to the fluorescence quenching of FDCN. The detection limit of FDCN for Fe^{3+} was 0.26 μM, and the selectivity and sensitivity to Fe^{3+} were not affected by the metal ions Ni^{+}, Pb^{2+}, Mg^{2+}, Li^{+}, Cd^{2+}, Ba^{2+}, Cu^{2+}, Co^{2+}, Zn^{2+}, Mn^{2+}, Ag^{+} and Fe^{2+}. Job's plot analysis showed the association stoichiometry between FDCN and Fe^{3+} to be 1 : 1 and an association constant of $3.23 \times 10^{4}\ M^{-1}$ calculated by the Benesi–Hilderbrand equation. The high hydrophilicity, low cytotoxicity, high sensitivity, and selectivity of FDCN for Fe^{3+} qualified the chemosensor for Fe^{3+} trace detection in drinking water and biology.

Conflicts of interest

There are no conflicts to declare.

References

1 N. Abbaspour, R. Hurrell and R. Kelishadi, *J. Res. Med. Sci.*, 2014, **19**, 164–174.
2 Y. J. Ding, H. Zhu, X. X. Zhang, J. J. Zhu and C. Burda, *Chem. Commun.*, 2013, **49**, 7797–7799.
3 H. T. Steinmetz, A. Tsamaloukas, S. Schmitz, J. Wiegand, R. Rohrberg, J. Eggert, F. Breuer, H. W. Tessen, H. Eustermann and L. Thomas, *Support. Care Cancer*, 2011, **19**, 261–269.
4 W. A. Jefferies, D. L. Dickstein and M. Ujiie, *J. Alzheim. Dis.*, 2001, **3**, 339–344.
5 J. L. Hamilton and J. N. Kizhakkedathu, *Molecular and Cellular Therapies*, 2015, **3**, 1–15.
6 M. R. Gallego and L. E. Díaz, *J. Am. Assoc. Lab. Anim. Sci.*, 2020, **59**, 17–23.
7 M. R. Pourjavid, A. A. Sehat, M. Arabieh, S. R. Yousefi, M. H. Hosseini and M. Rezaee, *Mater. Sci. Eng., C*, 2014, **35**, 370–378.
8 G. A. Antunes, H. S. dos Santos, Y. P. da Silva, M. M. Silva, C. M. S. Piatnicki and D. Samios, *Energy Fuels*, 2017, **31**, 2944–2950.
9 S. E. Pepper, M. Borkowski, M. K. Richmann and D. T. Reed, *Anal. Chim. Acta*, 2010, **663**, 172–177.
10 A. Trokourey, B. Aka and T. Diaco, *Ann. Chimie Sci. Matériaux*, 2003, **28**, 177–191.
11 T. Pivetta, S. Masuri, M. G. Cabiddu, C. Caltagirone, A. Pintus, M. Massa, F. Isaia and E. Cadoni, *New J. Chem.*, 2019, **43**, 12032–12041.
12 E. Bozkurt, M. Arik and Y. Onganer, *Sens. Actuators, B*, 2015, **221**, 136–147.
13 W. Yin, H. Cui, Z. Yang, C. Li, M. She, B. Yin, J. Li, G. Zhao and Z. Shi, *Sens. Actuators, B*, 2011, **157**, 675–680.
14 Z. Chen, X. Xu, D. Meng, H. Jiang, Y. Zhou, S. Feng, Z. Mu and Y. Yang, *J. Fluoresc.*, 2020, **30**, 1007–1013.
15 Q. P. Zhang, T. B. Wei, J. N. An, Y. Y. Chen, G. F. Gong, Q. Zhou, H. L. Yang, H. Yao, Y. M. Zhang and Q. Lin, *Supramol. Chem.*, 2019, **31**, 745–755.
16 X. Z. Sun, D. Moon, T. Yagishita and T. Minowa, *Trans. ASABE*, 2013, **56**, 1061–1067.
17 L. Y. Song, Y. Z. Wu, X. X. Pei, R. Li, H. T. Chen and X. Z. Sun, *Inhalation Toxicol.*, 2020, **32**, 388–401.
18 X. Z. Sun, Q. He and Y. Yang, *J. Renewable Mater.*, 2020, **8**, 447–460.
19 J. L. Huang, C. J. Li and D. G. Gray, *ACS Sustainable Chem. Eng.*, 2013, **1**, 1160–1164.
20 T. Abitbol, A. Palermo, J. M. Moran-Mirabal and E. D. Cranston, *Biomacromolecules*, 2013, **14**, 3278–3284.

21 T. Leng, Z. J. Jakubek, M. Mazloumi, A. C. W. Leung and L. J. Johnston, *Langmuir*, 2017, **33**, 8002–8011.
22 X. Z. Sun, Y. H. Xue, J. Y. Li, Y. Yang, Y. Bai and Y. J. Chen, *RSC Adv.*, 2021, **11**, 24694–24701.
23 Q. Ding, J. Zeng, B. Wang, W. Gao, K. Chen, Z. Yuan and J. Xu, *Carbohydr. Polym.*, 2017, **175**, 105–112.
24 L. Zhang, Q. Li, J. Zhou and L. Zhang, *Macromol. Chem. Phys.*, 2012, **213**, 1612–1617.
25 H. Chen, J. Huang, B. Hao, B. Yang, S. Chen, G. Yang and J. Xu, *Carbohydr. Polym.*, 2019, **224**, 115198.
26 B. L. Xue, Y. Yang, R. Tang, Y. C. Sun, X. F. Cao, P. Y. Li, Z. Zhang and X. P. Li, *Cellulose*, 2020, **27**, 729–742.
27 G. F. Chen, H. M. Jia, L. Y. Zhang, J. Hu, B. H. Chen, Y. L. Song, J. T. Li and G. Y. Bai, *Res. Chem. Intermed.*, 2012, **39**, 4081–4090.
28 J. Yao, W. Dou, W. Qin and W. Liu, *Inorg. Chem. Commun.*, 2009, **12**, 116–118.
29 S. Warrier and P. S. Kharkar, *Spectrochim. Acta, Part A*, 2018, **188**, 659–665.
30 Y. J. Zhang, X. Z. Ma, L. Gan, T. Xia, J. Shen and J. Huang, *Cellulose*, 2018, **25**, 5831–5842.
31 M. Acar, E. Bozkurt, K. Meral, M. Arık and Y. Onganer, *J. Fluoresc.*, 2015, **157**, 10–15.
32 Y. Zhang, G. Wang and J. Zhang, *Sens. Actuators, B*, 2014, **200**, 259–268.
33 Z. Zhang, S. Lu, C. Sha and D. Xu, *Sens. Actuators, B*, 2015, **208**, 258–266.
34 H. Wang, X. Ye and J. Zhou, *Nanomaterials*, 2019, **9**, 279.
35 L. Wang, H. Zhu, G. Xu, X. Hou, H. He and S. Wang, *J. Mater. Chem. C*, 2020, **8**, 11796–11804.
36 Z. Liu, M. Chen, Y. Guo, J. Zhou, Q. Shi and R. Sun, *Chem. Eng. J.*, 2020, **384**, 123260.
37 Bio-Rad Laboratories, Inc. Infornatics Division, *The Sadtler Handbook of Infrared Spectra*, 2004.
38 V. Arjunan, N. Puviarasan, S. Mohan and P. Murugesan, *Spectrochim. Acta, Part A*, 2007, **67**, 1290–1296.
39 G. I. Jones, W. R. Jackson, C. Choi and W. R. Bergmark, *J. Phys. Chem.*, 1985, **89**, 294–300.
40 D. Cao, Z. Liu, P. Verwilst, S. Koo, P. Jangjili, J. S. Kim and W. Lin, *Chem. Rev.*, 2019, **119**, 10403–10519.